Current driven dynamics of domain walls constrained in ferromagnetic nanopillars

Matteo Franchin,[1,2,*] Thomas Fischbacher,[2] Giuliano Bordignon,[1,2] Peter de Groot,[1] and Hans Fangohr[2]
[1]*School of Physics and Astronomy, University of Southampton, Southampton SO17 1BJ, United Kingdom*
[2]*School of Engineering Sciences, University of Southampton, Southampton SO17 1BJ, United Kingdom*
(Received 24 April 2008; revised manuscript received 12 July 2008; published 29 August 2008)

We investigate the effects of an electric current on the domain wall formed inside a cylindrical ferromagnetic nanopillar as a consequence of the pinning of the magnetization at its ends. We first present the results of three-dimensional and one-dimensional micromagnetic simulations and show that the system approaches a stationary equilibrium, where the domain wall is compressed in the direction of the electron flow and rotates around the nanopillar axis with constant frequency in the microwave frequency range. We obtain the dependence of the rotation frequency on the length of the nanopillar and on the magnitude of the applied current density. We then introduce a one-dimensional analytical model and find a formula for the rotation frequency in two current regimes: a low current regime, where the frequency is linearly proportional to the current density and a high current regime, where the frequency is quadratically proportional to the current density. Good agreement is found with the results of the simulations. The system may have possible applications as a nanosized microwave generator, which could operate without external magnetic fields and whose emission frequency could be controlled by a dc current.

DOI: 10.1103/PhysRevB.78.054447 PACS number(s): 75.60.Ch, 72.25.Ba, 75.75.+a

I. INTRODUCTION

The interaction between electric currents and domain walls in ferromagnetic nanowires has been the subject of intensive study in recent years. Experiments have shown that a spin polarized current can produce a domain-wall movement in the direction of the electron flow.[1–4] This effect has been investigated analytically and numerically.[5–7] In a recent work[8] we studied the case where a domain wall occurs inside a ferromagnetic nanopillar as a consequence of the pinning of the magnetization at the nanopillar ends. The situation is similar to the one which occurs for a domain wall in a nanowire, with an important difference: The domain wall is pinned and cannot translate freely along the nanopillar. For such a system one may expect a compression of the domain wall, rather than a translation. Micromagnetic simulations confirm this expectation, showing that the applied current produces a compression of the domain wall in the direction of the electron flow. More surprisingly the system reaches a stationary equilibrium characterized by a rotation of the compressed domain wall around the nanopillar axis with frequency which is constant in time and lies within the microwave frequency range. This behavior is not found for domain walls in nanowires and suggests novel technological applications: Such a system may be used to obtain microwaves emission from a dc electric current without the need for an external magnetic field.

In this paper, we study how the rotation frequency depends on the applied current density and on the nanopillar length. We first present the results of three-dimensional and one-dimensional micromagnetic simulations. We then introduce an analytical model and find two current regimes: the low current regime, where the frequency depends linearly on the current density, and the high current regime, where the dependence becomes quadratic. We derive approximate formulae for the frequency in these two regimes and find good agreement with the results from the simulations. The analytical model supports the numerical results and gives more insight on the physics of the system.

II. SYSTEM

The system under investigation is a ferromagnetic nanopillar in the shape of a cylinder, as shown in Fig. 1. The magnetic moments at the right and left faces of the cylinder are assumed to be pinned, pointing to the right at the right face and to the left at the left face. As a consequence, a domain wall is developed. The system may thus approximate the situation we considered in a previous work,[8] where a nanopillar made of a magnetically soft material was sandwiched between two magnetically hard layers and the pinning was provided by the exchange coupling at the soft-hard interfaces. In this paper, however, we do not make any assumptions on the origin of the pinning, which can be achieved in other ways. One example could be a ferromagnetic body, made by two regions connected through a small constriction: A domain wall is developed in the constriction, when the wider regions are magnetized in opposite directions.[9,10]

In this work we study how the constrained domain wall reacts to a uniform and constant electric current flowing along the axis of the nanopillar. Both the simulations and the analytical investigations we present are based on a micromagnetic model, where the interaction between the spins of the conduction electrons and the magnetization is taken into account using the Zhang and Li correction to the Landau-Lifshitz-Gilbert equation:[6]

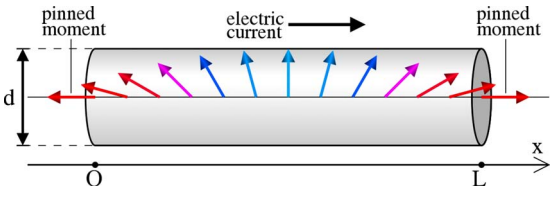

FIG. 1. (Color online) A sketch of the system. The arrows on the cylinder axis represent the magnetization, pinned in opposite directions at the nanopillar ends.

$$\partial_t \mathbf{M} = -\gamma \mathbf{M} \times \mathbf{H} + \frac{\alpha}{M_s} \mathbf{M} \times \partial_t \mathbf{M} - \frac{v}{M_s^2} \mathbf{M} \times (\mathbf{M} \times \partial_x \mathbf{M}) - \frac{\xi v}{M_s} \mathbf{M} \times \partial_x \mathbf{M}. \quad (1)$$

In this equation $\mathbf{M}$ is the magnetization, $M_s = \|\mathbf{M}\|$ is the saturation magnetization, $\mathbf{H}$ is the effective magnetic field, γ is the gyromagnetic ratio, α is the damping parameter and we use the notation $\partial_t \equiv \frac{\partial}{\partial t}$, $\partial_x \equiv \frac{\partial}{\partial x}$. The current density j is applied in the positive x direction and enters the model through the parameter $v = \frac{Pj\mu_B}{eM_s(1+\xi^2)}$, where P is the degree of polarization of the spin current, μ_B is the Bohr magneton, e is the absolute value of the electron charge, $\xi = \tau_{ex}/\tau_{sf}$ is the ratio between the exchange relaxation time and the spin-flip relaxation time. In our model M_s is uniform in space and constant in time. We can then obtain an explicit form for Eq. (1):

$$\partial_t \mathbf{m} = -\gamma' \mathbf{m} \times \mathbf{H} - \gamma' \alpha \mathbf{m} \times (\mathbf{m} \times \mathbf{H}) - a v' \mathbf{m} \times (\mathbf{m} \times \partial_x \mathbf{m}) - \bar{a} v' \mathbf{m} \times \partial_x \mathbf{m}, \quad (2)$$

where $\mathbf{m} = \mathbf{M}/M_s$ and $\gamma' = \gamma/(1+\alpha^2)$, $v' = v/(1+\alpha^2)$. The two dimensionless coefficients a and $\bar{a}$ are $a = 1 + \alpha\xi$ and $\bar{a} = \xi - \alpha$.

The effective field $\mathbf{H}$ receives two main contributions: one from the exchange interaction, the other from the magnetostatic interaction. The exchange interaction tries to keep neighboring moments aligned. The exchange field is $\mathbf{H}_{exch} = C\partial_x^2 \mathbf{m}$, where $C = \frac{2A}{\mu_0 M_s}$, A is the exchange coupling constant of the material and $\partial_x^2 \equiv \frac{\partial^2}{\partial x^2}$. The magnetostatic interaction mainly tries to align $\mathbf{M}$ with the axis of the nanopillar (when its length is much greater than its radius), thus reducing the magnetic surface charges.

The model neither includes the effects of Joule heating nor the effects of the Oersted field. We discuss these assumptions in Sec. VI.

III. THREE-DIMENSIONAL MICROMAGNETIC SIMULATIONS

For the micromagnetic simulations we use NMAG,[11] a finite element method (FEM) micromagnetic simulation package. The cylindrical nanopillar is modeled by a three-dimensional unstructured mesh and first-order FEM is used to discretize the space. The time evolution of the magnetization is calculated using Eq. (2), except for the sites which lie on the left and right faces of the nanopillar. For these sites we assume $\partial_t \mathbf{m} = 0$, which corresponds to infinitely strong pinning on the magnetization. The magnetostatic field is calculated using the hybrid FEM/boundary element method (BEM) method.[12,13] We use material parameters of permalloy: $M_s = 0.8 \times 10^6$ A/m, $A = 1.3 \times 10^{-11}$ A/m and $\xi = 0.01$. The damping constant is chosen to be $\alpha = 0.02$. This value was estimated for permalloy in a previous work.[14] The applied magnetic field is zero for all the simulations presented in this paper.

We first consider a nanopillar with length $L = 40$ nm and diameter $d = 20$ nm. The simulation starts from an initial magnetization configuration, which is obtained by preliminarily relaxing the system with $j_P = 0$ and is shown in Fig. 3(a). A polarized current with density $j_P = Pj = 10^{11}$ A/m^2 is then applied at time $t = 0$ along the positive x direction, meaning that the conduction electrons flow in the opposite direction.

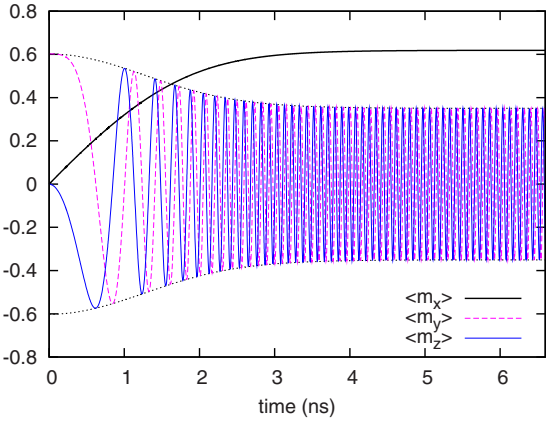

FIG. 2. (Color online) The evolution of the components of the average normalized magnetization $\langle \mathbf{m} \rangle = \langle \mathbf{M} \rangle / M_s$ as a function of time. The nanopillar length is $L = 40$ nm.

The simulation shows that the domain wall compresses along the direction of the electron flow. In Fig. 2 the components of the normalized spatially averaged magnetization $\langle \mathbf{m} \rangle = \langle \mathbf{M} \rangle / M_s$ are plotted as functions of time up to 6.6 ns. The x component of $\langle \mathbf{m} \rangle$ is initially zero, reflecting the symmetry of the initial configuration [Fig. 3(a)] for inversions $x \to -x$. The current gradually pumps energy into the system and compresses the domain wall against the left face of the nanopillar [Fig. 3(b)]. In the opposite side of the nanopillar the magnetization aligns along the positive x axis, resulting in an increase in $\langle m_x \rangle$. The compression is accompanied by a rotation of the whole domain wall around the axis of the nanopillar, as can be seen clearly by looking at behavior of the y and z components of $\langle \mathbf{m} \rangle$ in Fig. 2. To obtain the rotation frequency we express $\langle \mathbf{m} \rangle$ in spherical coordinates where x is chosen as the polar axis. The frequency is then calculated numerically as $\nu = |\partial_t \phi|/2\pi$, where ϕ is the azimuth angle. In the case we are considering here, where the current points in the direction of the positive x axis, the sign

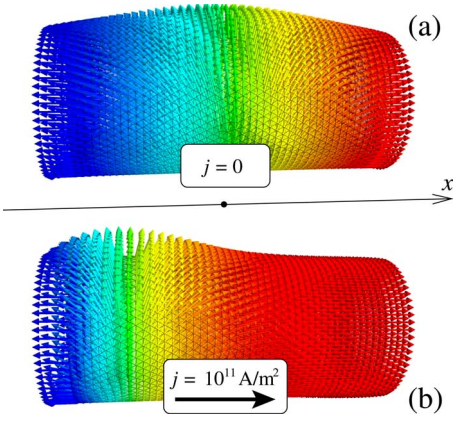

FIG. 3. (Color online) The magnetization configuration for the simulation of Fig. 2 is shown at $t = 0$ ns (a) and $t = 6.6$ ns (b).

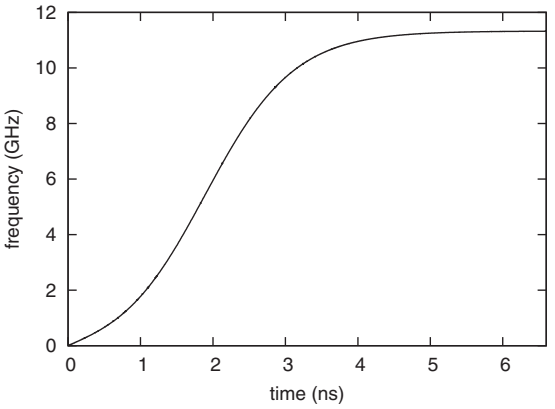

FIG. 4. The time dependence of the frequency for the rotation of the domain wall around the x axis for a three-dimensional micromagnetic simulation of a nanopillar with $L=40$ nm.

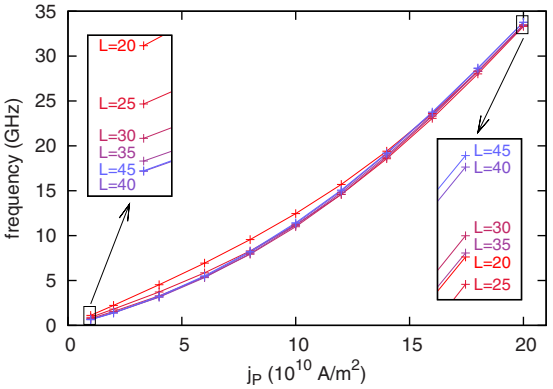

FIG. 5. (Color online) The frequency as a function of j_P for different nanopillar lengths L, as obtained from three-dimensional micromagnetic simulations.

of $\partial_t \phi$ is negative and indicates a left-handed rotation around the same axis (or equivalently a right-handed rotation around the negative x axis, which is actually the compression direction). The rotation frequency is initially zero and increases monotonically toward a maximum asymptotical value ν_f, as shown in Fig. 4.

To determine ν_f we let the simulation proceed up to the point where the variation in time of the frequency becomes lower than a given threshold. In particular we stop the simulation when $\Delta\nu/\Delta t$ becomes lower than 0.01 GHz/ns. The variation $\Delta\nu/\Delta t$ is calculated with $\Delta t=100$ ps. The simulation then proceeds up to $t_f=6.6$ ns and the asymptotical frequency is found to be $\nu_f \approx \nu(t=t_f)=11.3$ GHz (at 11 ns the frequency is only 0.004 GHz higher, which corresponds to an increase of 0.04%).

The asymptotical dynamics is characterized by a rotation around the x axis, without deformation of the domain wall. In such a state, the total energy of the system is constant in time and hence the energy dissipated by the damping term must be exactly balanced by the energy pumped in by the applied current.

Further simulations are performed to find the exact dependence of the frequency on the polarized current density j_P and on the length of the nanopillar L. A different mesh is considered for each different value of L. All the meshes are obtained meshing a cylinder with diameter $d=20$ nm and are generated such that their simplices have edge lengths lower than 2.6 nm (on average their edges are around 1.2 nm long).

The graph in Fig. 5 shows the asymptotic frequency ν_f obtained repeating the simulation for $j_P=1,2,4,\ldots,18,20 \times 10^{10}$ A/m^2 and for $L=20,25,\ldots,45$ nm. The figure shows that while the frequency changes considerably with the current density j_P, there are small differences between the curves obtained for different nanopillar lengths L. In particular the curves for different values of L overlap, showing that this parameter has different effects for different current regimes: For currents around 10^{10} A/m^2, the highest rotation frequency is reached by the shortest nanopillar, while for currents around 2×10^{11} A/m^2 the highest frequency is reached by the longest nanopillar.

IV. ONE-DIMENSIONAL MICROMAGNETIC SIMULATIONS

We repeat the simulations discussed in Sec. III for a simplified model, where the nanopillar is represented by a one-dimensional magnetic string. Such a study has a twofold purpose: On the one hand, it provides data for a comparison with the three-dimensional model, which allows to better understand the effects of the nanopillar shape and size. On the other hand, it gives insight on the limitations of one-dimensional models, such as the one presented in Sec. V.

For the one-dimensional simulations we use the same material parameters and the same procedure as in Sec. III. The three-dimensional meshes are, however, replaced by one-dimensional meshes with 0.5 nm spacing between neighboring nodes. This one-dimensional model neglects the inhomogeneities of the magnetization in the plane orthogonal to the nanopillar axis and—more importantly—it neglects the contribution of the magnetostatic field.

The results of the simulations are shown in Fig. 6. We study the system for $L=20,25,\ldots,60$ nm and for the same values of j_P as in Sec. III. The curves for different nanopillar lengths are more clearly spaced with respect to the three-dimensional case and show that to a longer nanopillar corresponds a lower rotation frequency. This result is reasonable for such a one-dimensional system, where the width of the domain wall is just L: to a smoother change of the magnetization corresponds a reduced spin-transfer torque effect. In the three-dimensional system, things are different. The magnetostatic field pulls the magnetization along the axis of the nanopillar to reduce the magnetic charges at the surface. This is an additional pinning effect which keeps the width of the domain wall from growing for larger values of L. In other words, in the three-dimensional system the domain-wall width does not depend on L, if L is large enough. Then the frequency does not depend on L either.

In Fig. 6 we see that the frequencies for $L=20$ nm obtained in the one-dimensional model are close to the ones obtained in the full three-dimensional model. This seems to suggest that the magnetostatic effects become less important in shorter nanopillars.

V. ANALYTICAL MODEL

We investigate the system with a one-dimensional analytical micromagnetic model. The purpose of such a study is to support the micromagnetic simulations and to give a better understanding of the physics of the system. The model does not include the magnetostatic field and assumes it does not qualitatively affect the physics of the system. We begin by writing Eq. (2) in spherical coordinates:

$$\partial_{\tau'}\theta = 2\cos\theta\partial_u\theta\partial_u\phi + \sin\theta\partial_u^2\phi + \alpha[\partial_u^2\theta - \sin\theta\cos\theta(\partial_u\phi)^2] + Va\partial_u\theta + V\bar{a}\sin\theta\partial_u\phi, \tag{3a}$$

$$\partial_{\tau'}\phi\sin\theta = \alpha[2\cos\theta\partial_u\theta\partial_u\phi + \sin\theta\partial_u^2\phi] - \partial_u^2\theta + \sin\theta\cos\theta(\partial_u\phi)^2 - V\bar{a}\partial_u\theta + Va\sin\theta\partial_u\phi. \tag{3b}$$

Only dimensionless quantities appear in these equations: $u = \frac{x}{L}$, $\tau' = \frac{\gamma' C}{L^2}t$, $V = \frac{L}{\gamma C}v$. We want the magnetization to point to the left at the left boundary and to the right at the right boundary:

$$\theta(u=0) = \pi, \quad \theta(u=1) = 0, \tag{4}$$

which are boundary conditions for our system of differential equations. When the current is zero, $V=0$, the equilibrium (such that $0 = \partial_{\tau'}\theta = \partial_{\tau'}\phi$) is obtained for

$$\theta(u) = \pi(1-u), \quad \phi(u) = \text{const}, \tag{5}$$

as can be seen with a substitution in Eqs. (3a) and (3b). For $V>0$, computer simulations show that the system approaches a stationary equilibrium where the whole magnetization rotates with constant frequency around the axis of the nanopillar. We then investigate the case where there is no further compression of the domain wall, while it could still rotate with constant angular velocity around the x axis:

$$\partial_{\tau'}\theta = 0, \quad \partial_{\tau'}\phi = \Omega' = \text{const}. \tag{6}$$

The rotation frequency can be obtained from Ω' through the relation $\nu_f = \frac{\gamma' C}{2\pi L^2}|\Omega'|$.

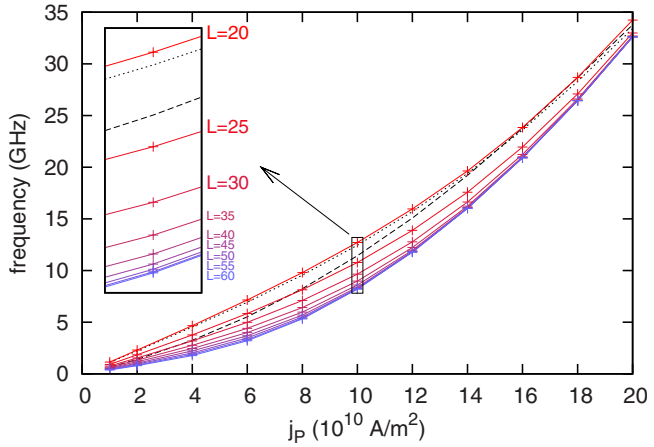

FIG. 6. (Color online) The frequency as a function of j_P for different nanopillar lengths L, as obtained from one-dimensional micromagnetic simulations. The dotted and dashed curves show the results obtained for the three-dimensional system (Fig. 5) in the case $L=20$ and $L=45$, respectively.

As a first try to find such a solution we assume $\partial_u\phi = 0$ and find the corresponding compression profile from Eq. (3a):

$$\alpha\partial_u^2\theta + Va\partial_u\theta = 0.$$

Solving this equation we get

$$\partial_u\phi = 0, \quad \theta(u) = \pi\frac{e^{\lambda(1-u)} - 1}{e^{\lambda} - 1},$$

where $\lambda = \frac{Va}{\alpha}$. However this is not a solution of Eqs. (3a) and (3b), as can be easily verified with a substitution in the second equation of this system:

$$-\partial_u^2\theta - V\bar{a}\partial_u\theta \neq \Omega'\sin\theta.$$

We conclude that $\partial_u\phi$ cannot be neglected. It is then important to understand the role of $\partial_u\phi$, the torsion of the domain wall produced as an effect of the flow of the electric current.

We point out that the rotation is a consequence of the compression of the domain wall and—in this sense—can be thought to be an indirect effect of the spin-transfer torque. This can be seen clearly by considering the zero-current equilibrium configuration [Eq. (5)] and looking at the derivatives of θ and ϕ with respect to the reduced time τ', when a current density is immediately applied (this is the situation which occurs at $t=0$ in the simulations). Equation (3a) becomes $\partial_{\tau'}\theta = -Va\pi$, which suggests that a compression of the domain wall is going to take place. Equation (3b) becomes $\sin\theta\partial_{\tau'}\phi = V\bar{a}\pi$. We have found a direct contribution to the rotation of the domain wall. This contribution, however, is suppressed by the factor $V\bar{a} \sim -5\times10^{-4}$, which is rather small for the materials and the range of current densities we are interested in ($j=10^{11}$ A/m^2, $V\sim5\times10^{-2}$). We conclude that the domain wall initially compresses without significant rotation and torsion. The compression, however, leads to nonvanishing values for the term $\partial_u^2\theta$ and this in turn requires nonvanishing values for $\sin\theta\partial_{\tau'}\phi$, as can be seen by looking at Eq. (3b). In summary, the compression of the domain wall (i.e., $\partial_u^2\theta \neq 0$) produces a torsion and rotation of the domain wall (i.e., $\sin\theta\partial_{\tau'}\phi \neq 0$).

We now proceed by rearranging Eqs. (3a) and (3b) and imposing Eq. (6):

$$-\Omega \sin\theta = \partial_u^2\theta - \sin\theta\cos\theta(\partial_u\phi)^2 + V\xi\partial_u\theta - V\sin\theta\partial_u\phi, \tag{7a}$$

$$\alpha\Omega \sin\theta = 2\cos\theta\partial_u\theta\partial_u\phi + \sin\theta\partial_u^2\phi + V\partial_u\theta + V\xi\sin\theta\partial_u\phi. \tag{7b}$$

We have here introduced $\Omega = \Omega'/(1+\alpha^2)$. We note that at the boundaries of the nanopillar ($u=0,1$) Eq. (7b) gives

$$\theta = \pi,\ 0 \rightarrow \partial_u\theta\left(\partial_u\phi \mp \frac{V}{2}\right) = 0.$$

$\partial_u\theta$ cannot be zero at the boundaries, at least for small currents, for which we expect the solution to be close to the zero-current solution [Eq. (5)]. We then conclude:

$$\partial_u\phi|_{u=0} = +\frac{V}{2}, \quad \partial_u\phi|_{u=1} = -\frac{V}{2}.$$

This result suggests that $\partial_u\phi$ should be of the same order of V. This is an assumption we make, which enables us to proceed with important approximations. Indeed, for the material and the geometry we are dealing with, and a current density around $j \sim 10^{11}$ A/m^2, we have $V \sim 0.05$. Therefore, the assumption $\partial_u\phi \sim V$ implies that the typical torsion of the domain wall is, in general, rather small: $\Delta\phi \approx V \approx 3°$. It implies also that the second and fourth terms on the right-hand side of Eq. (7a) are of order $V^2 \approx 2.5\times10^{-3}$. On the other hand, Eq. (5) suggests that $\partial_u\theta \sim -\pi$ and we expect $\partial_u^2\theta$ to be on the same order of magnitude, when the domain wall is compressed. We may then neglect terms of order V^2 and terms of order ξV, since typically $\xi \sim 10^{-2}$. Then the system [Eqs. (7a) and (7b)] reduces to

$$-\Omega \sin\theta = \partial_u^2\theta, \tag{8a}$$

$$\alpha\Omega \sin\theta = 2\cos\theta\partial_u\theta\partial_u\phi + \sin\theta\partial_u^2\phi + V\partial_u\theta. \tag{8b}$$

We immediately note that all the terms containing ξ have disappeared from the system: We are neglecting the nonadiabatic effects of the spin-transfer torque interaction.

Equation (8a) is the pendulum equation. It could be used together with the boundary conditions [Eq. (4)] to obtain $\theta(u)$, once Ω is known. However, determining Ω is not easy. We can find a constraint on Ω and θ from the second Eq. (8b), by multiplying both of its sides by $\sin\theta$,

$$\alpha\Omega \sin^2\theta = \partial_u[\sin^2\theta\partial_u\phi] - V\partial_u\cos\theta. \tag{9}$$

This equation can be integrated:

$$\int_0^1 \sin^2\theta \mathrm{d}u = -\frac{2V}{\alpha\Omega}. \tag{10}$$

$\theta(u)$ can now be found by searching for the solutions of pendulum Eq. (8a) which also satisfy Eqs. (4) and (10). Our main goal, however, is to find $\Omega(V)$, rather than finding $\theta(u)$ and $\phi(u)$. To do this, we multiply both sides of Eq. (8a) by $\partial_u\theta$:

$$\Omega\partial_u\cos\theta = \frac{1}{2}\partial_u(\partial_u\theta)^2,$$

which can be integrated, obtaining

$$\Omega\cos\theta + I = \frac{1}{2}(\partial_u\theta)^2,$$

where I is a positive (take $\theta=\pi/2$) integration constant. This equation gives an expression for $\partial_u\theta$:

$$\partial_u\theta = -\sqrt{2(I+\Omega\cos\theta)}. \tag{11}$$

The sign in front of the square root was chosen in order to satisfy the boundary conditions [Eq. (4)]. We can now change variable of integration in Eq. (10), obtaining

$$\int_0^\pi \frac{\sin^2\theta \mathrm{d}\theta}{\sqrt{2(I+\Omega\cos\theta)}} = -\frac{2V}{\alpha\Omega}. \tag{12}$$

A second integral equation can be derived integrating the identity $\mathrm{d}\theta/\partial_u\theta = \mathrm{d}u$ and using the boundary conditions [Eq. (4)]:

$$\int_0^\pi \frac{\mathrm{d}\theta}{\sqrt{2(I+\Omega\cos\theta)}} = 1. \tag{13}$$

I and Ω can then be found by solving the following system of equations:

$$f_1\left(\frac{\Omega}{I}\right) = -\frac{2V}{\alpha\Omega}\sqrt{I},$$

$$f_2\left(\frac{\Omega}{I}\right) = \sqrt{I}, \tag{14}$$

where the two functions f_1 and f_2 are defined in the following way:

$$f_1(x) = \int_0^\pi \frac{\sin^2\theta \mathrm{d}\theta}{\sqrt{2(1+x\cos\theta)}},$$

$$f_2(x) = \int_0^\pi \frac{\mathrm{d}\theta}{\sqrt{2(1+x\cos\theta)}},$$

and x has to be such that $|x|<1$ in order for f_2 to exist. System (14) is difficult to solve in general. Here we consider two limiting cases: (i) $|\frac{\Omega}{I}| \gtrsim 0$. Since $f_1(0) = \frac{\pi}{2\sqrt{2}}$ and $f_2(0) = \frac{\pi}{\sqrt{2}}$, we get $I = \frac{\pi^2}{2}$ and $\Omega \approx -\frac{4V}{\alpha}$. The condition $|\frac{\Omega}{I}| \gtrsim 0$ becomes then $|\frac{V}{\alpha}| \ll \frac{\pi^2}{8}$; (ii) $|\frac{\Omega}{I}| \lesssim 1$. Since $f_1(1) = \frac{4}{3}$, $\Omega \approx -\frac{3}{2}\frac{V}{\alpha}\sqrt{I}$. Considering that $|I| \approx |\Omega|$, we finally get $\Omega \approx -(\frac{3}{2}\frac{V}{\alpha})^2$. Moreover, when $x \rightarrow 1$, $f_2(x) \rightarrow +\infty$. We then conclude that $|I| \approx |\Omega| \gg 1$ and hence $|\frac{V}{\alpha}| \gg 1$.

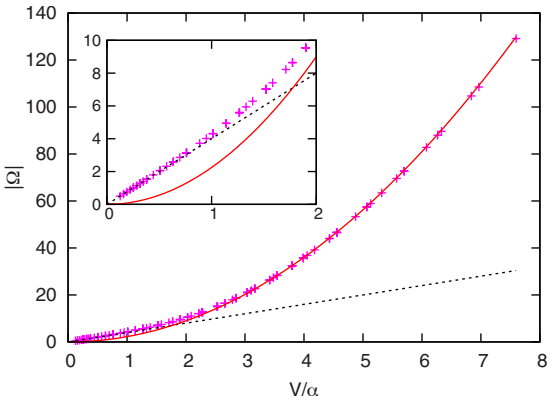

FIG. 7. (Color online) Comparison between the numerical values for $|\Omega(V)|$ obtained from the one-dimensional micromagnetic simulations (crosses) and the low current (dotted line) and high current (solid line) analytical solutions.

These results are summarized below:

$$\Omega = \begin{cases} -\dfrac{4V}{\alpha} & \text{for } \left|\dfrac{V}{\alpha}\right| \ll 1 \\ -\left(\dfrac{3}{2}\dfrac{V}{\alpha}\right)^2 & \text{for } \left|\dfrac{V}{\alpha}\right| \gg 1. \end{cases} \tag{15}$$

The frequency can be deduced easily from the formula $\nu_f = \frac{\gamma' C}{2\pi L^2}|\Omega'| = \frac{\gamma C}{2\pi L^2}|\Omega|$:

$$\nu_f = \begin{cases} \dfrac{2}{\pi}\dfrac{v}{\alpha L} & \text{for } \left|\dfrac{Lv}{\alpha\gamma C}\right| \ll 1 \\ \dfrac{1}{2\pi\gamma C}\left(\dfrac{3}{2}\dfrac{v}{\alpha}\right)^2 & \text{for } \left|\dfrac{Lv}{\alpha\gamma C}\right| \gg 1. \end{cases} \tag{16}$$

Let us now define j_0 such that $V/\alpha = j_P/j_0$. Then the low current condition $|\frac{V}{\alpha}| \ll 1$ becomes $|j_P| \ll j_0$ and similarly the high current condition becomes $|j_P| \gg j_0$ and,

$$j_0 = \frac{2e\gamma}{\mu_0\mu_B}\frac{\alpha(1+\xi^2)A}{L}, \tag{17}$$

which shows, in particular, that the critical current which distinguishes between the low current regime and the high current regime depends on the nanopillar length L.

We note that in the low current regime the frequency does not depend on the strength of the exchange interaction $C = 2A/\mu_0 M_s$. It depends on the length of the domain wall L and on the magnitude of the applied current v. On the other hand, in the high current regime, the frequency does not depend on L anymore. It depends however on the strength of the exchange coupling C and depends quadratically on v.

Figure 7 shows the validation of the analytic expressions for $\Omega(V)$ against the results of the one-dimensional micromagnetic simulations of Fig. 6. The graph contains all the data shown in Fig. 6 plotted in terms of the reduced quantities V and Ω. Consequently, all the points obtained for different values of L and j_P lie in a single curve. The graph shows good agreement between theory and simulations, thus supporting the approximations which were made to get to the final formulas.

We make a final remark on the different dependence of the frequency on the applied current in the two regimes. There are two reasons why an increase in the current may lead to an increased asymptotic frequency. First, the two terms through which the spin-transfer torque enters Eq. (1) share the prefactor $v \propto j$: double the current, double the spin-transfer torque terms and double the effect. The second way the current may increase the frequency is by reducing the domain-wall width. A reduced domain-wall width corresponds to an increased value of $\partial_x \mathbf{M}$, which appears in both the spin-transfer torque terms. In the linear regime, only the first effect occurs. Indeed, from Eq. (11) we see that $\partial_u\theta = -\sqrt{2I}\sqrt{1+\frac{\Omega}{I}\cos\theta}$, where $\frac{\Omega}{I} \approx 0$ and $I = \frac{\pi^2}{2}$. We then get $\partial_u\theta \approx -\pi$, which means that, in the low current regime, the domain-wall shape does not change too much with respect to the zero-current configuration [Eq. (5)]. On the other hand, in the high current regime, $\frac{\Omega}{I} \approx -1$ and $\partial_u\theta = -\frac{3V}{\alpha}\sin\frac{\theta}{2}$. $\partial_u\theta$ depends on j, through V. This analysis suggests that the low/high current regimes correspond, respectively, to low/high domain-wall deformation.

VI. DISCUSSION AND CONCLUSION

We discussed the role of the nanopillar shape in a previous work:[8] Due to the cylindrical shape of the nanopillar, a rotation of the whole magnetization around the nanopillar axis does not require to overcome any energy barriers. This feature is extremely important for the dynamic process we have studied in this paper, because it allows the current to gradually transfer energy to the system and store it by compressing the domain wall. An important question to answer is then: how much does the shape of the nanopillar affect the dynamics of such systems? We have cross performed simulations for nanopillars with a square section and found very similar results: For a nanopillar with length $L=40$ nm and square section 20×20 nm we chose $j=10^{10}$ A/m^2 and found a frequency $\nu_f \approx 0.61$ GHz, while for the corresponding cylindrical nanopillar $\nu_f = 0.64$ GHz.

Equations (15) and (16) show that the rotation frequency can be expressed as a function of V/α and ultimately as a function of j_P/α. This means that for a value of α larger by a factor two, a current density larger by a factor two is required in order to obtain the same frequency. This consideration indicates that low damping constant is a desirable feature, when choosing a material for a concrete realization of the system proposed in this paper. We have chosen permalloy, because, besides being a particularly soft magnetic material, it has been intensively studied in spin transport experiments in recent years and values between 0.01 and 0.02 have been estimated[14–16] for its damping constant α. We point out that our choice, $\alpha=0.02$, is conservative: The value $\alpha=0.01$ would lead to considerably enhanced current effects and—in the quadratic regime—would lead to quadrupled frequency.

The electric currents required in spin-transfer torque experimental studies are often high enough to produce considerable Joule heating and Oersted field. These effects should, however, be expected to become less and less important as the system is scaled down. Indeed, smaller systems are able to dissipate heat more efficiently than big systems, since re-

duced size corresponds to increased surface/volume ratio. Similarly, the Oersted field is reduced in smaller nanowires, being proportional to the total current flowing throughout the sample. On the other hand, the spin-transfer torque does not depend on the system size, provided the current density remains constant. These considerations suggest that the nanopillar we presented in this paper should be even less affected than the larger nanowires studied in other works,[2,4,16] where Oersted field and Joule heating were found to be negligible or unable to limit the effects of spin-transfer torque. Besides these empirical arguments, we can obtain an estimate of the Oersted field, using a simple model, where the nanowire is approximated with an infinitely long cylinder with radius R and is traversed by a uniform current density j. In this simple picture, the Oersted field circulates around the nanopillar axis and has maximum intensity $B_{\max}=\mu_0 Rj/2$, which is reached on the surface of the nanopillar. Considering the extreme case $j_P=2\times10^{11}$ A/m^2 and $P=0.4$, we get $j=5\times10^{11}$ A/m^2 and $B_{\max}=0.00314$ T. This field does not act against the rotation of the whole magnetization around the nanopillar axis, since it is invariant for such transformations. Moreover, its intensity is so small that we cannot really expect any relevant deformations of the artificial domain wall created by the pinning (the demagnetizing field is 2 orders of magnitude bigger and still produces only moderate profile adjustments). We conclude that neglecting the Oersted field is an appropriate approximation.

In summary, we used micromagnetic simulations to study the spin-transfer torque effects that occur in a nanopillar when the magnetization is pinned at its ends. We showed that the dynamics of such a system is characterized by a stationary precession of the whole magnetization of the system around its axis. We presented both three-dimensional and one-dimensional computations and studied the asymptotical precession frequency ν_f as a function of the polarized current and of the nanopillar length. We derived an analytical model which provides further insight into the physics of the system and shows that there are two current regimes, where the system exhibits different dependencies on the applied current. We found good agreement between the results of the simulations and the theory.

ACKNOWLEDGMENTS

This work was funded by the Engineering and Physical Sciences Research Council (EPSRC) in the United Kingdom (Grants No. GR/T09156, No. GR/S95824, and No. EP/E040063).

*franchin@soton.ac.uk

[1] A. Yamaguchi, T. Ono, S. Nasu, K. Miyake, K. Mibu, and T. Shinjo, Phys. Rev. Lett. **92**, 077205 (2004).
[2] M. Kläui, P.-O. Jubert, R. Allenspach, A. Bischof, J. A. C. Bland, G. Faini, U. Rüdiger, C. A. F. Vaz, L. Vila, and C. Vouille, Phys. Rev. Lett. **95**, 026601 (2005).
[3] M. Hayashi, L. Thomas, Y. B. Bazaliy, C. Rettner, R. Moriya, X. Jiang, and S. S. P. Parkin, Phys. Rev. Lett. **96**, 197207 (2006).
[4] G. Meier, M. Bolte, R. Eiselt, B. Krüger, D.-H. Kim, and P. Fischer, Phys. Rev. Lett. **98**, 187202 (2007).
[5] Z. Li and S. Zhang, Phys. Rev. B **70**, 024417 (2004).
[6] S. Zhang and Z. Li, Phys. Rev. Lett. **93**, 127204 (2004).
[7] G. Tatara and H. Kohno, Phys. Rev. Lett. **92**, 086601 (2004).
[8] M. Franchin, G. Bordignon, T. Fischbacher, G. Meier, J. P. Zimmermann, P. de Groot, and H. Fangohr, J. Appl. Phys. **103**, 07A504 (2008).
[9] P. Bruno, Phys. Rev. Lett. **83**, 2425 (1999).
[10] H. Fangohr, J. P. Zimmermann, R. P. Boardman, D. C. Gonzalez, and C. H. de Groot, J. Appl. Phys. **103**, 07D926 (2008).
[11] NMAG—a micromagnetic simulation environment, 2007, http://nmag.soton.ac.uk/
[12] D. R. Fredkin and T. R. Koehler, IEEE Trans. Magn. **26**, 415 (1990).
[13] D. A. Lindholm, IEEE Trans. Magn. **20**, 2025 (1984).
[14] Y. Nakatani, A. Thiaville, and J. Miltat, Nat. Mater. **2**, 521 (2003).
[15] J. P. Nibarger, R. Lopusnik, and T. J. Silva, Appl. Phys. Lett. **82**, 2112 (2003).
[16] B. Krüger, D. Pfannkuche, M. Bolte, G. Meier, and U. Merkt, Phys. Rev. B **75**, 054421 (2007).